Geophysical Journal International

Geophys. J. Int. (2011) doi: 10.1111/j.1365-246X.2011.05150.x

Lithospheric structure beneath the Zagros collision zone resolved by non-linear teleseismic tomography

Z. Hossein Shomali,[1,2] Forough Keshvari,[1] Jamshid Hassanzadeh[3] and Noorbakhsh Mirzaei[1]

[1] *Institute of Geophysics, University of Tehran, Tehran,* 14155-6466, *Iran. E-mail: Hossein.Shomali@geo.uu.se*
[2] *Department of Earth Sciences, Uppsala University, Uppsala,* 752 36, *Sweden*
[3] *Tectonics Observatory, California Institute of Technology, Pasadena, CA* 91125, *USA*

Accepted 2011 July 11. Received 2011 July 11; in original form 2010 April 6

SUMMARY

The upper-mantle structure across the Zagros collision zone, in southwest Iran, is investigated using a non-linear weighted damped least-squares teleseismic tomography approach. The resolution of the structures/transitions in the upper mantle is enhanced significantly by correcting the teleseismic relative arrival time residuals for an *a priori* crustal velocity model and then performing the inversion with fixed crustal blocks. To investigate whether or not the lithospheric blocks and major transitions in the resulting model are required by the data or are artefacts of the inversion, the data were inverted using two different inverse methods (singular value decomposition and a quadratic programming method). New high-quality seismic velocity models show apparent correlation between surface geological features and seismic velocity structures at lithospheric depth across the Zagros collision zone. The image shows a sharp lithospheric boundary at the Main Zagros Thrust between 100 km and 250 km depth with *P*-wave velocity about 3 per cent faster within the Arabian Shield to the south. A step-like increase in lithospheric thickness across the Zagros collision zone is assumed to separate two different mantle structures namely the Arabian (to the south) and the Eurasian (to the north) domains. The most striking feature resolved is a north-dipping slab-like positive velocity anomaly.

Key words: Body waves; Seismic tomography; Continental tectonics: compressional.

1 INTRODUCTION

The Zagros orogenic system in Iran is the location of a young continent–continent collision between the Arabian and Eurasian plates. Surface uplift and shallow seismicity indicate that the crust is still being actively deformed. Plate history in Iran pertaining to this study begins in the Late Cretaceous when the Zagros open marine carbonate shelf (i.e. the passive margin of Arabia) approached a complex island arc system in the younger Neotethys ocean or the Semail supra-subduction oceanic plate of Stampfli & Borel (2004). The arc–continent collision resulted in several massive ophiolite obductions. This north-dipping ophiolitic belt delineates the present day border between the Zagros fold-thrust belt (ZFTB, see Fig. 1) and the Sanandaj-Sirjan metamorphic zone (SSZ). Subduction of the oceanic plate, however, continued under Iran (i.e. Eurasia active margin) and resulted in more continental magmatism in SSZ and formation of younger arcs of Urumieh-Dokhtar (UDMA) and the Alborz, in the northern part of Iran, through a complex arc migration history in Late Cretaceous-Tertiary times. Consumption of the oceanic lithosphere separating the Zagros from SSZ was arguably finalized in the Miocene and since then tectonic deformation has changed to continent–continent collision mode.

Most of the Zagros collision system along the studied traverse can be divided into five lithotectonic belts (Fig. 1, e.g. Stöcklin 1968). From southwest, these are (1) the ZFTB (Koyi 1988), (2) the Zagros Thrust Zone (ZTZ) characterized by the highest elevations in entire Zagros range, (3) the Zagros main reverse fault, often named Main Zagros Thrust (MZT) with the Oman-type ophiolites on its NE side which correspond to the Late Cretaceous–Early Tertiary arc–continent collision, (4) the SSZ representing largely plutonic level of the Mesozoic arc and forearc basin and (5) the Central Iran continental block with a dominantly Eocene arc known as UDMA on its southern margin.

Active subduction still occurs to the south and southwest of Turkey, beneath the Cyprian and Hellenic arcs, respectively, and to the southeast of Iran, beneath the Makran (Maggi & Priestley 2005). Active subduction of the continental crust of the Arabian shield beneath the Zagros region was postulated by many studies based on the existence of subcrustal earthquakes (depth >50 km) (e.g. Nowroozi 1971; Kadinsky-Cade & Barazangi 1982;

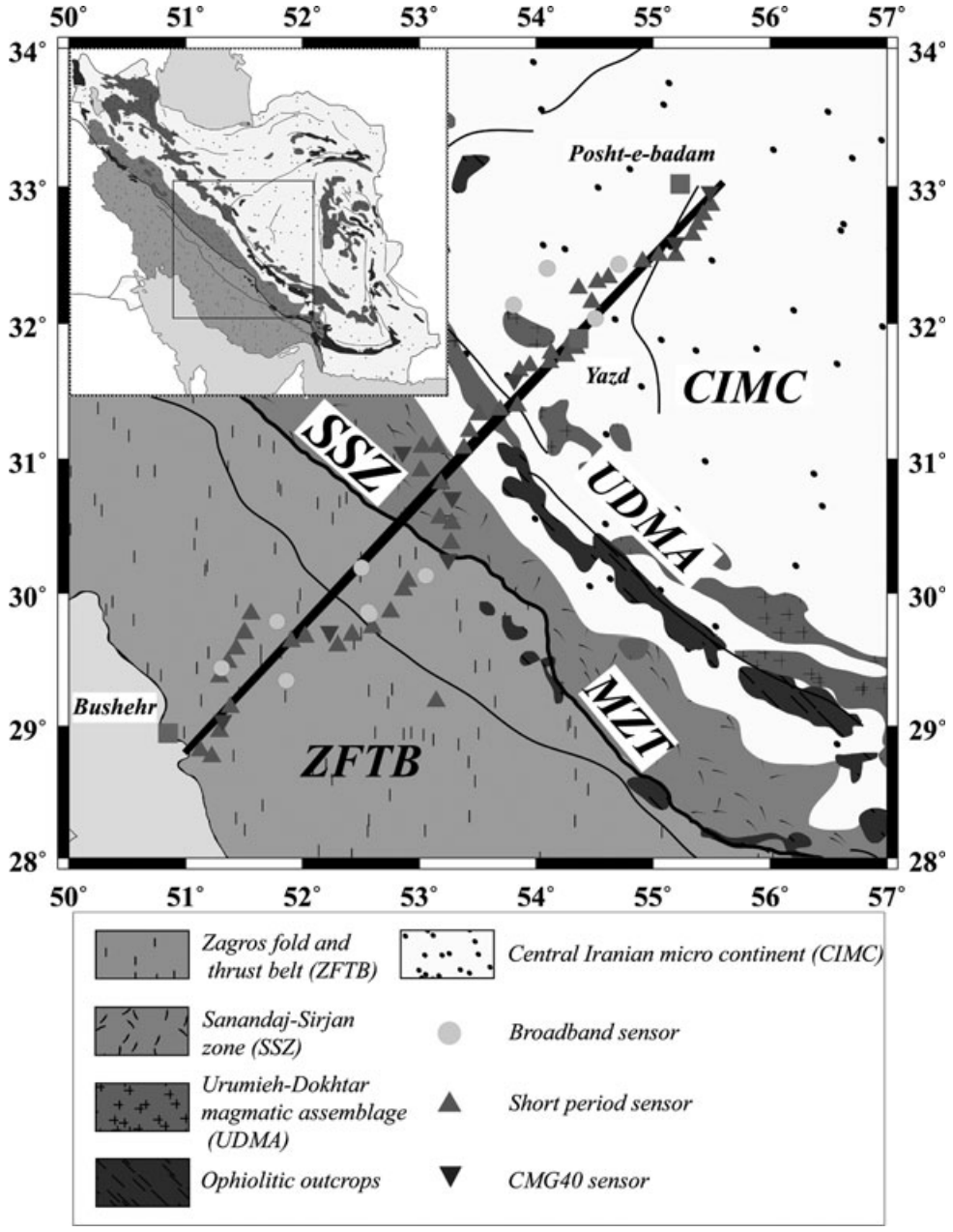

Figure 1. Simplified tectonic map of the studied area slightly modified from Kaviani *et al.* (2007). The profile utilized to compute all cross-sections (from Bushehr to Posht-e-Badam) is depicted by a thick line. Key: MZT, Main Zagros Thrust; ZFTB, Zagros Fold and Thrust Belt; SSZ, Sanandaj-Sirjan Metamorphic Zone; UDMA, the Urumieh-Dokhtar Magmatic Arc; CIMC, Central Iran Micro-continent.

Moores & Twiss 1995). However, the occurrence of the upper-mantle seismicity in the Zagros region has been ruled out by many authors asserting that most of the seismicity in the upper mantle is caused by mis-location of earthquakes which are actually rupturing in the upper crust (e.g. Maggi *et al.* 2000; Engdahl *et al.* 2006).

For a better understanding of the geodynamic setting of the Zagros suture, robust imaging of the seismic velocities in the upper mantle is required. Several key questions still exist on the upper-mantle structures of the Zagros collision zone that could not be adequately answered by mere geological tools. However, seismic tomography can effectively reflect on issues including the present state of the subducted oceanic slab, whether it is connected or detached and if lithospheric delamination has occurred or not. Answers to those questions have also bearing on the long debated tectonic issues such as the timing and location of collision. To investigate the upper-mantle structure/transition across the Zagros collision zone (see Fig. 1), a teleseismic traveltime tomography approach was used to image the structures primarily in the depth range of 70–460 km using a passive seismic experiment conducted from 2000 November to 2001 April and coordinated by Iranian (from the International Institute of Earthquake Engineering and Seismology, Tehran) and French (from LGIT, Grenoble) seismologists.

Two different *P*-phase data sets are available based on the Zagros passive experiment. The data set used by Kaviani *et al.* (2007) contained earthquakes at teleseismic distances and different azimuths including offline earthquakes with respect to the SW–NE axis of the profile. The relative arrival time residuals were then inverted for *P*-wave velocity of the upper 250 km of the model including the

crust. Thus no crustal correction was applied to the input data set *a priori* to inversion. The inversion was also conducted based on a linear scheme. Here, the inversion result of the second data set is presented. In this new data set, we picked 41 high-quality teleseismic wave fronts with magnitudes larger than m_b 5.5 and epicentral distances between 30–90°. Because of the rather linear distribution of the stations, and because the axis of the profile is approximately perpendicular to the major tectonic features in the area, primarily teleseismic earthquakes with great circle paths roughly in line with the SW–NE axis of the profile were considered. Limiting the data set in this manner can alleviate possible complications related to significant 3-D structures.

2 DATA COMPILATION

Geological evidence and earlier geophysical studies indicate that the large-scale lithospheric structure in the studied area should be reasonably 2-D, for example, parallel to the trend of the Zagros mountains (Fig. 1). Therefore the passive experiment was designed as linear network perpendicular to the Zagros mountains. 66 seismic stations (11 broad-band, 8 medium band and 47 short-period instruments) were deployed in a SW–NE network along a 620-km-long by 100-km-wide strip across the Zagros collision zone (for further information about the experiment, see e.g. Paul *et al.* 2006; Kaviani *et al.* 2007).

41 high-quality seismic events were selected for the teleseismic tomography study. These events, shown in Fig. 2, are located inline with respect to the axis of the profile (N40°E). Generally, the signal-to-noise ratio of the *P*-wave signals is higher in the northern part of the profile (Central Iran) than in the southern part (Zagros), where the sedimentary cover is thicker. Earthquake locations were taken from the event catalogue reported by USGS and corrected as reported by Engdahl *et al.* (1998). All seismograms were restituted to simulate a short-period WWSSN SP station (the World Wide Standardized Seismographic Network) with a dominant frequency of 1 Hz (Oliver & Murphy 1971).

The earliest readable peak or trough of the *P* phase was first picked on a trace with relatively high signal-to-noise ratio (reference station) for each selected earthquake (see Fig. 3). Then by overlaying the waveform of the so-called reference station on the other traces the relative position of the peak or trough with respect to the reference station was picked. This process reduces complexities caused by changes in the details of the *P* waveform as it traverses the profile and avoids cycle skipping (e.g. Evans & Achauer 1993; Shomali *et al.* 2002). For each event–station pair, the theoretical arrival times were then calculated based on the iasp91 global 1-D reference earth model (Kennett & Engdahl 1991). The arrival time residuals were then calculated by subtraction of the calculated theoretical arrival times from the observed phases. For each selected event, the relative arrival time residuals were finally calculated by subtracting the associated mean for each event from the arrival time residuals. By removing the mean of the arrival time residuals for each recorded event, the source and propagation path traveltime anomalies due to lower-mantle effects are discarded from the data since all rays traverse the lower mantle essentially along the same ray path (Dueker *et al.* 1993; Evans & Achauer 1993). In other words, it was assumed that the traveltime residuals generated outside the given target volume are approximately constant across the seismic profile (Masson & Trampert 1997). However, there is still a risk of projecting the deeper mantle velocity anomalies into the target model (Masson & Trampert 1997).

The resulting data set of relative arrival time residuals can be used to image the structure of the upper mantle with high resolution by backprojecting the incoming rays to estimate the size and magnitude of velocity anomalies (Aki *et al.* 1977). The nature of the observed data, which have been demeaned for a global mean

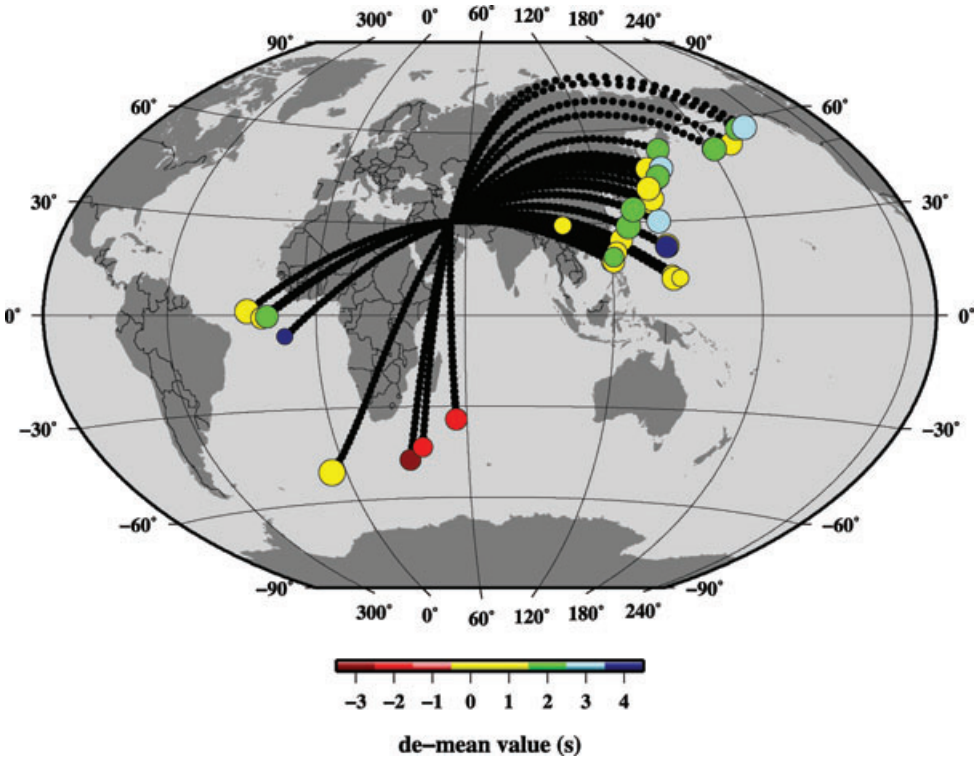

Figure 2. Distribution of the earthquakes used in this study. Colours refer to the amount of 'de-mean value' traveltime for different earthquakes.

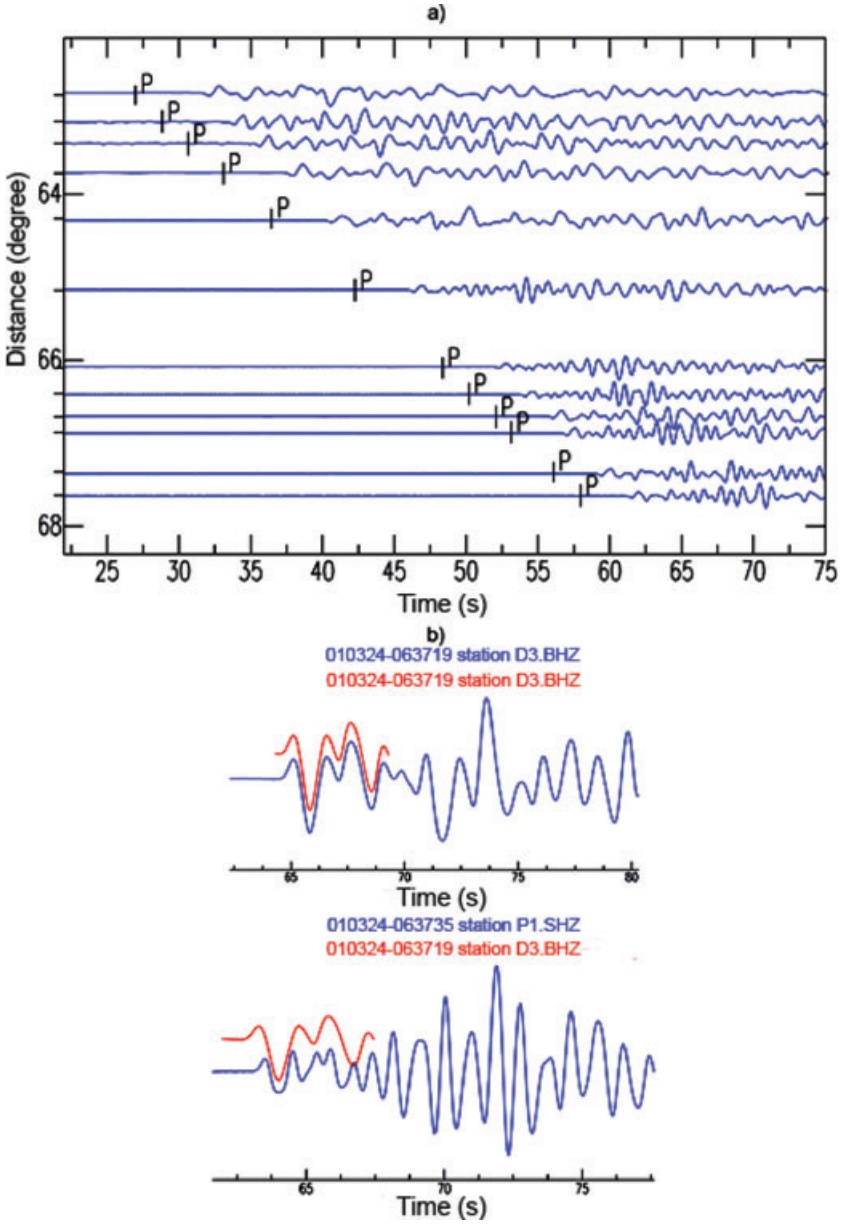

Figure 3. (a) An example of the data record section for the event of 2001 March 24, 06:27 UTC that occurred at 34.11°N and 132.54°E with a magnitude of 6.8 M_W. The *P* arrival times are computed based on the iasp91 traveltime model. (b) An example of the relative picking process on two selected waveforms. Top panel: the waveform obtained at the reference station D3. Bottom panel: overlaid waveform of the reference station D3 (red line) on the readable peak of another station, P1 (blue line).

model, does not allow estimation of the absolute velocity anomalies within the target area. It is normally considered that this limitation is caused by using relative arrival times which may still contain minor sources of error and bias in the analysis, for example, related to propagation of signals from the source to the (limited) volume of the model (Evans & Achauer 1993). The inverted model can thus be considered to reflect deviations about some unknown average earth model with meaningful velocity contrasts. Although the forward modelling is done within a known background model, the final velocity perturbations resulting from the inversion cannot be considered relative to the known background model, due to the nature of the relative arrival time residuals. However, for a large enough target volume, the layer-average velocities can be considered close to some commonly accepted 1-D background/reference model (Lévêque & Masson 1999). These layer-average velocities can then be considered close enough to the correct regional structure (e.g. Sandoval *et al.* 2004). In this study, the iasp91 traveltime model (Kennett & Engdahl 1991) was used as a starting model in the inversion. The processing and phase picking were done using the Seismic Analysis Code (SAC, Lawrence Livermore National Laboratory 2010) and Seismic Handler software (Stammler 1993).

3 MODEL PARAMETRIZATION

The Earth volume beneath the Zagros profile was parametrized with a 3-D grid with a lateral grid size of 50 × 50 km^2 in the horizontal direction and 16 layers from the surface of the Earth down to a depth of 460 km (see Fig. 4). The grid spacing in vertical direction varies between 20 km at shallow depths, and 40 km below 120 km depth

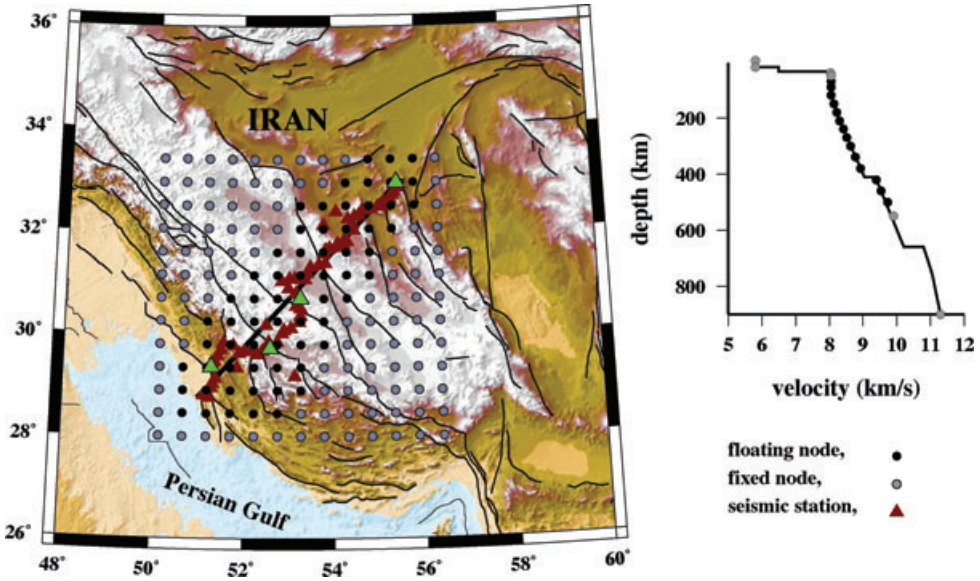

Figure 4. Model parameters (horizontal grid distribution and layers) used in the inversion are shown overlaid on a coloured relief map of Iran. The velocities of the starting nodes are taken from the iasp91 model (Kennett & Engdahl 1991). The velocities of the floating nodes are determined in the inversion. The average crustal traveltime corrections (in seconds) applied to the stations marked in green are listed in Table 1.

(Fig. 4) with an additional layer at 900 km depth for stability of the inversion. Model parameters between neighbouring grid nodes were determined by a linear interpolation scheme (Steck & Prothero 1991). Fixed nodes are those fixed in the inversion, while floating nodes are those inverted for velocity anomalies. The total number of model parameters is 4275, with 1014 floating model parameters. The initial velocities of the nodes are taken from the iasp91 model of Kennett & Engdahl (1991). The grid size chosen provides a high resolution to delineate the structures in the upper mantle and produces a smoothing effect, because it is larger than the minimum resolvable structure based on the dominant frequency content of the data.

4 CRUSTAL CORRECTION

The error associated with teleseismic traveltime residuals is usually lower than the traveltime perturbations caused by crustal structure. Previous studies (see e.g. Shomali *et al.* 2002; Lippitsch *et al.* 2003; Shomali *et al.* 2006; Eken *et al.* 2007; Eken *et al.* 2008) suggested that crustal structures have a derogatory effect on the structures resolved in the upper mantle. This effect can significantly be reduced by correcting the observed data based on a crustal model obtained from other geophysical data (e.g. Lippitsch *et al.* 2003).

A complete 3-D crustal information for the studied area is not available, thus we decided to use crust 2.0 (Bassin *et al.* 2000) for the crustal correction. Traveltime variations due to the crustal model were then calculated for each event–seismic station pair based on a simplex-based ray tracer algorithm (Steck & Prothero 1991). A cross-section along the Zagros profile of the crustal model is depicted in Fig 5(a).

If the crustal model used in the inversion is correct, then the tomographic results for upper mantle will be enhanced. There could, also, be a risk of introducing some bias into our results, if some errors or inadequacies exist in the crustal model. There are uncertainties in the available data used to construct the crustal model, and geographical interpolation between existing data is necessary to produce the crustal model. Therefore, various tests comparing the inversions with and without crustal corrections were carried out. Application of crustal corrections does not change the general trends of observed residuals and tests show that resolution for the upper-mantle structures is enhanced when the crustal correction is applied. The average crustal traveltime corrections (s) applied to the four stations along the Zagros profile are presented in Table 1. We conclude that it is advisable to apply the crustal corrections, and that future results might be further improved when more information about crustal structure becomes available (e.g. Shomali *et al.* 2002; Lippitsch *et al.* 2003; Eken *et al.* 2007).

The elevation also varies greatly along the Zagros profile (see Fig. 5c) thus it was necessary to correct the observed *P*-phase relative arrival time residuals prior to the inversion for variations due to the elevation along the profile. The correction was done by ray tracing the target model to zero elevation and then to the true elevation, and then adding the corresponding time to the measured data.

5 INVERSION RESULTS

Inversion was carried out based on a non-linear ACH (Aki, Christoffersson and Husebye) tomography method (Aki *et al.* 1977; Weiland *et al.* 1995). According to the ACH method the relative residuals are inverted to estimate the size and magnitude of the velocity deviations within the volume below the receiver region. The ray tracing was conducted using a simplex-based method for computing the 3-D minimum traveltime ray paths (Steck & Prothero 1991; Weiland *et al.* 1995). To estimate the solutions to the non-linear problem an iterative-weighted damped least-squares method (e.g. Shomali *et al.* 2002) was implemented. A singular value decomposition (SVD) method was also used to calculate the inverse of the data kernel (a matrix of partial derivatives of traveltimes with respect to unknown velocity parameters). A data weighting matrix, proportional to the observation errors (e.g. Arlitt 1999; Shomali *et al.* 2002) and a model weighting matrix (corresponding to the spatial smoothing operator) were also implemented to stabilize the inversion processes. In each iteration, traveltime perturbations within the model were calculated. Normally, the inversion converges within

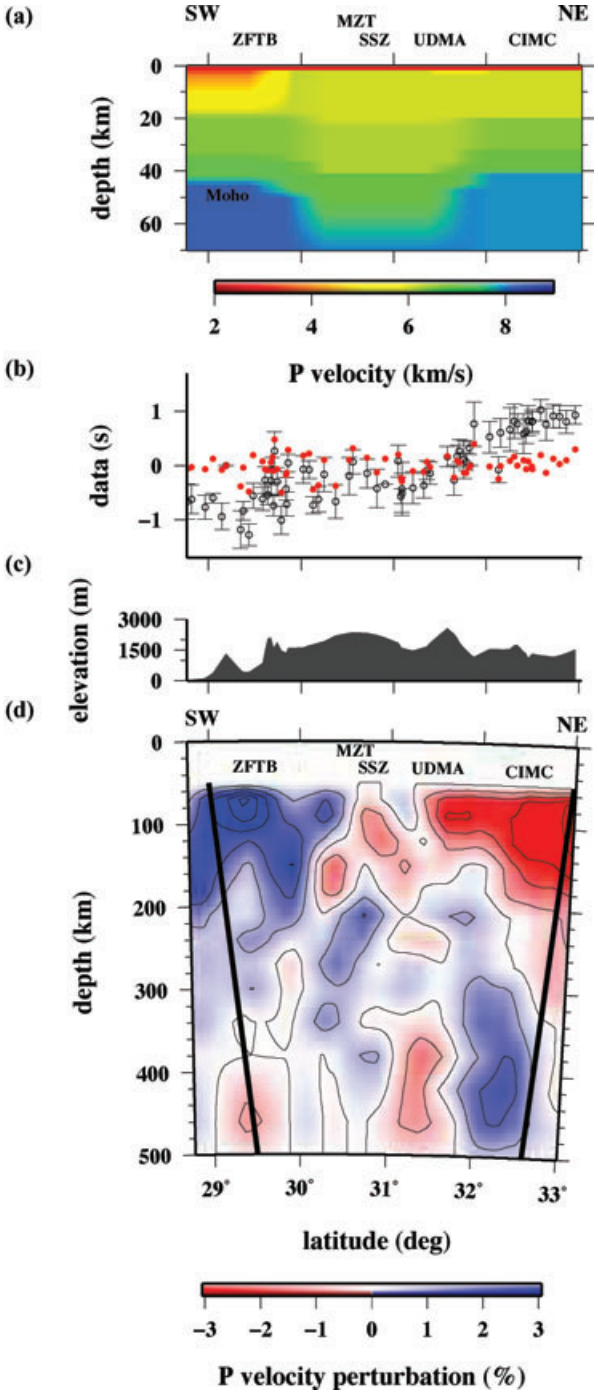

Figure 5. (a) A cross-section along the studied profile for the 3-D *P*-velocity crustal model. Location of the cross-section is shown in Fig. 1. (b) Observed relative arrival time residuals (black open circle) and relative residuals after iteration 3 (red dot) along the profile. (c) Elevation variations along the profile. (d) Smoothed inversion results after the third iteration. The results are shown as *P*-velocity deviations from the iasp91 (Kennett & Engdahl 1991) starting model. The two oblique lines limit the most reliable area of the results based on incidence angle of the seismic rays. Tectonic abbreviations as in Fig. 1.

four iterations. 1179 data points were used to invert the 1014 model parameters with a damping value of 120 s^2 per cent^{-2}. The optimum damping value was chosen based on the trade-off curve shown in Fig. 6(a). The damping factor directly affects the true number of

Table 1. The average crustal traveltime corrections (in seconds) applied to four stations along the Zagros profile. The corresponding stations are marked green in Fig. 4.

Stations	P1	F9	M4	M8
Latitude (°)	29.7	29.4	30.7	32.9
Longitude (°)	52.6	51.3	53.3	55.5
Residuals (s)	−0.4	−0.3	0.2	0.6

degrees of freedom in the inversion (e.g. Evans & Achauer 1993). To be confident that the tomographic model used is sufficiently deep (in relation to the length of the profile) and to ensure that no significant leakage occurs from structures below the model, initially the depth of the inverted model was taken to be about two-thirds of the aperture of the profile (e.g. Evans & Achauer 1993). The depth of the model was then fixed to 460 km based on the level of the variance reduction (normalized by the degrees of freedom) and also the geometry of the rays (Fig. 6b). Below this depth, rays diverge significantly and do not criss-cross, producing poor resolution (see Table 2, Cases I and II).

The result of the *P*-phase teleseismic tomography inversion is illustrated in Fig. 5(d) and is summarized in Table 2 (Case I). The figure shows velocity deviations from the iasp91 starting model, along the Zagros profile. Thus the blue and red regions can be directly assigned to the regions with higher and lower relative velocity. The well-resolved area in the inversion is confined by the two oblique lines that are calculated from incidence angles of the rays and the average *P*-velocity of the model (see 'Resolution Studies' section for more details). The observed residuals before inversion (black circles) and after the third iteration (red dots) are shown in Fig. 5(b). Note that the relative arrival time residuals shown are corrected for both the crustal and elevation effects. The data are demeaned and a clear trend is seen in the observed data which is due to the velocity variations in the upper mantle. According to the figure, the seismic stations in the southern part of profile show negative (early) arrival time residuals while those stations in the northern part have positive (delayed) residuals. Because of the near-vertical incident angles of the teleseismic rays the general trend of negative to positive relative arrival time residuals can be directly associated with areas of relatively high velocity in the south (Zagros) compared to the lower velocity in the north (Central Iran). The histograms of the residuals before and after the inversion are shown in Fig. 6(c). Note that the resulted model (Fig. 5d) after the inversion can explain about 79 per cent of the sum of the residuals (see Table 2). The histograms imply that a significant velocity contrast at depth is required to explain the data, consistent with our inverted images (see Fig. 5d).

Backazimuth variation of the relative arrival time residuals is shown in Fig. 7 for an extended data set which now includes earthquakes at teleseismic distances (between 30 to 90°) but from different azimuths with respect to the axis of the Zagros profile (N40°E). According to Fig. 7, no significant azimuthal dependency is observed for stations in the southern part, in ZFTB, and in the northern part of the profile, in Central Iran. However, some indications for azimuthal variations are observed in the central part of the profile, especially under SSZ and UDMA where the lithospheric structure is complex. In principle, our data cannot separate the effects of velocity heterogeneity from those of possible anisotropy. The interpretation of these images in terms of heterogeneities may be incorrect, as some of the observed velocity differences may be due to anisotropy rather than isotropic heterogeneity.

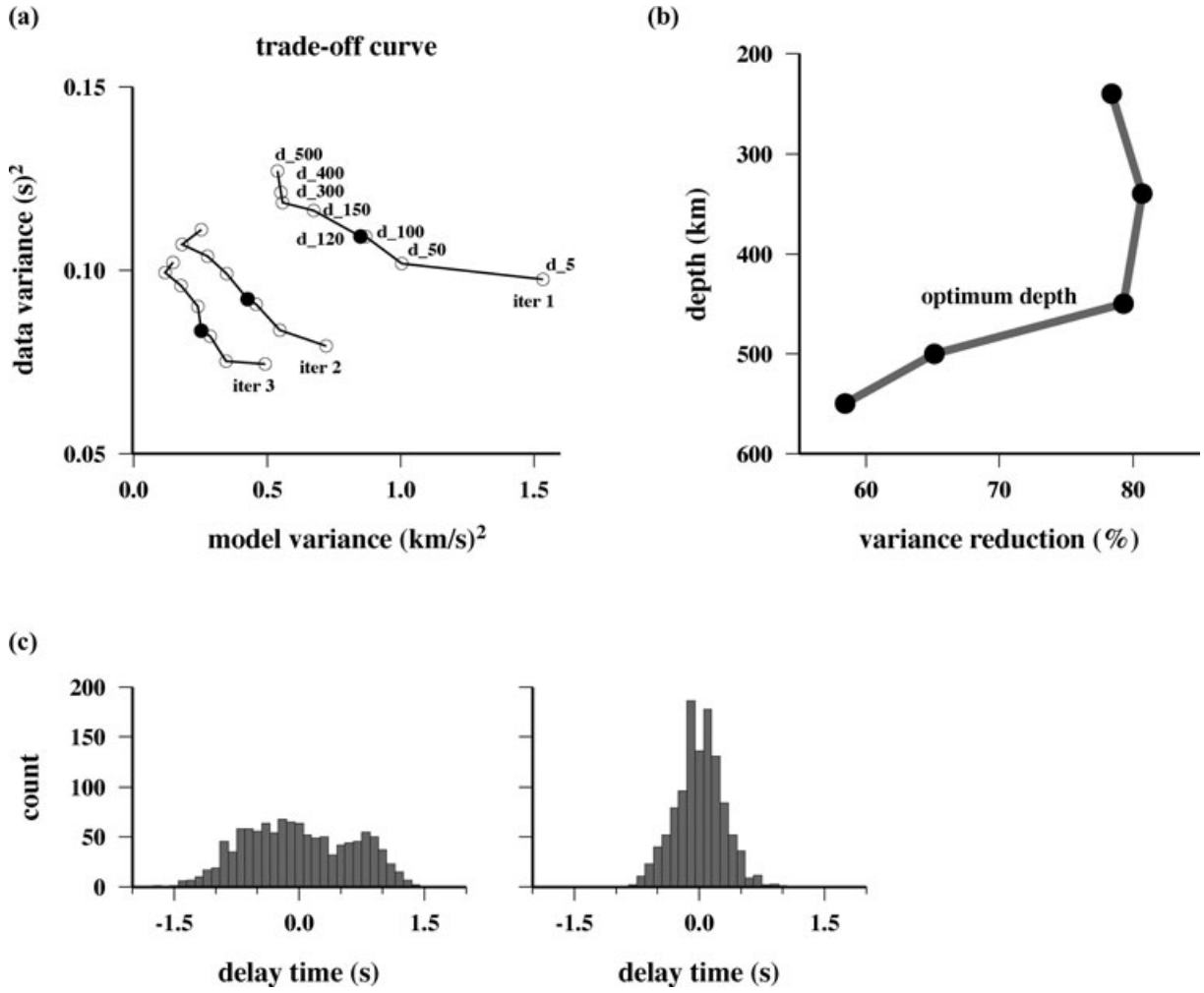

Figure 6. (a) Trade-off curve for different dampings and at three different iterations. Damping values from bottom to top are 5, 50, 100, 120, 150, 300, 400 and 500 s^2 per cent $^{-2}$. (b) Data variance reduction (normalized using the number of degrees of freedom in the model) as a function of inversion depth after the third iteration. Inversion depths are 240, 340, 460, 500 and 550 km, respectively. (c) Histograms of the data (traveltime residual sum) before (left-hand side) and after (right-hand side) the inversion.

Table 2. The inversion results.[a]

Case[b]	N	M	M_e[c]	Perturbation_model_length[c,d] (per cent)	Remaining_data_variance[c] $(s)^2$	Variance_reduction[c] (per cent)
Case I	1179	1014	871	3.9	0.08	79
Case II	1179	1092	944	3.7	0.14	65
Case III	1179	1088	935	3.1	0.13	72

N, M and M_e are no. of data, unknown model parameters and eigenvalues, respectively.
[a]Centre of the model: 30.7°N 53.3°E; error associated with data (s): 0.1; no. of events: 41; no. of seismic stations: 66; damping values for different cases: 120 s^2 per cent $^{-2}$.
[b]Case I: model depth of 460 km (the optimum solution); Case II: model depth of 500 km; Case III: model depth of 460 km, including the crustal layer in the inversion.
[c]Data are based on iteration no. 3.
[d]Perturbation_model_length is not normalized to the number of model parameters.

As a simple test of the possible bias due to inaccuracies in the crustal models, we also carried out an inversion with unconstrained crustal structure (Fig. 8 and Table 2, Case III). The results given in Table 2 also indicate that when the crustal model was not applied (Case III), and the inversion allowed estimation of even crustal structures, the perturbation in model length (per cent) decreases (as the number of model parameters in the inversion increases) and the remaining data variance (s^2) increases resulting in lower variance reduction (72 per cent) as compared to the inversion with crustal corrections (79 per cent variance reduction in Case I). The remaining ∼20 per cent data variance may be related to noise in the data. Therefore, comparing the inversions with and without crustal corrections indicates that the resolution for the upper-mantle structures is enhanced when the crustal correction is applied (see Figs 5d and 8 and Table 2). Major differences are observed in the middle of the profile where there is a significant change in Moho

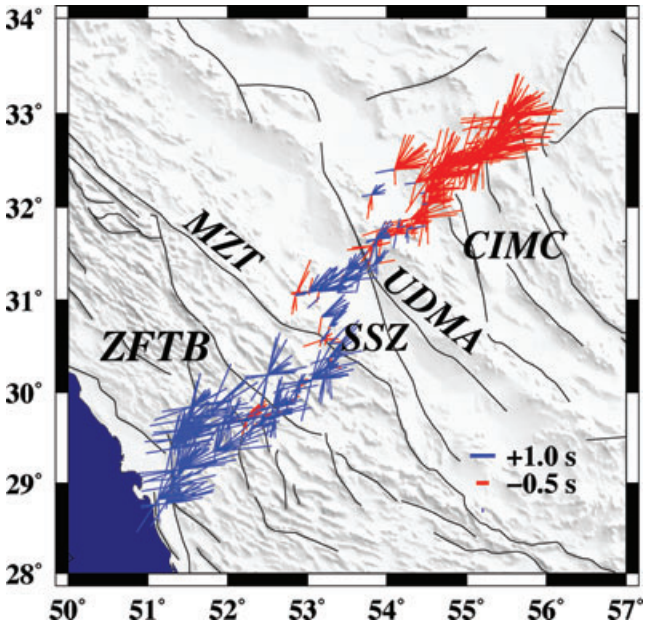

Figure 7. Backazimuth variation of the relative arrival time residuals for an extended data set (for more information see the text). Line lengths are proportional to the size of residuals, pointing towards the epicentre. Blue are early arrivals and red are late arrivals relative to the iasp91 (Kennett & Engdahl 1991) traveltime model.

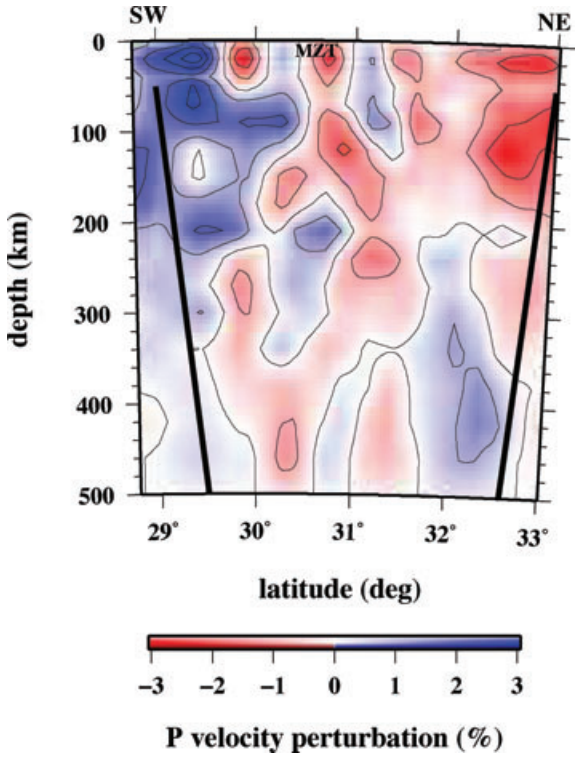

Figure 8. Inversion result for the case of a unconstrained crustal layer in the inversion.

depth (see Fig. 5a). While some of the details of the crustal model (see Fig. 5a) may not be completely correct, the major features, such as the dramatic deepening of Moho in the middle of the profile, are very well established, for example, using surface wave tomography method along the same profile determined by Shad Manaman & Shomali (2010). Other factors such as the effects of anisotropy etc. are very unlikely to have any radical effects on these major features (see e.g. inversion results in Table 2). We therefore conclude that any bias in our results due to the use of the crustal model is unlikely to be of major significance. Thus the crustal correction does enhance the upper-mantle structures and we base our interpretations on the corrected data.

6 RESOLUTION STUDIES

The resolution in teleseismic tomography experiments depends upon a number of factors including network configuration, period of operation, distribution in space of suitable sources, signal-to-noise ratio, model parametrization and the level of inhomogeneity within the relevant part of the Earth. A major problem in many tomographic inversions is an assessment of the reliability of the various features observed in the inverted model, not least because regularization parameters (such as damping, a threshold for dropping the eigenvalues, data and model weighting matrices) are needed to stabilize the solution. However, there is obviously a risk that the regularization, which is primarily a mathematical abstraction without a true physical or geological basis, may change some details in the solution. In this study the resolution of the model, resulting from the inversion, is validated using different measures as discussed later.

To find out whether or not the boundaries and blocks observed in the inverted model are required by the data, or are unconstrained or have been artificially caused by the inversion, the data are inverted using an alternative inversion method based on quadratic programming (QP, Parker 1980; Powell 1983; Schittkowski 2000; Shomali *et al.* 2002). QP is a well-established method in solving inverse problems, and its application to teleseismic tomography is discussed in detail by Shomali *et al.* (2002). One advantage of the method is that it facilitates the inclusion of inequality constraints into the inversion, which allows flexibly defined constraints to be included in the inversion to, for example, assess to what extent the data demand the inclusion of a particular feature in the model. The method was applied partly to see whether the application of a completely different inversion method reveals the same structures, or if some of these have been artificially caused by the inversion. Usually to stabilize the inversion process a number of regularization parameters including damping, spatial smoothing and eigenvalue rejection can be implemented. In the application of QP, we used the same symmetric positive-definite objective function as used for the SVD algorithm but without any spatial smoothing operator and due to the nature of the method no eigenvalue rejection was needed. The only requirement is now the lower and upper bounds of unknown model parameters, which were specified *a priori* to inversion to ± 3 per cent. This value was chosen based on the characteristics of previous inversions of the same data (SVD-part, Fig. 5d). The model obtained based on QP inversion is shown in Fig. 9(a). Note that no smoothing operator was imposed in the QP inversion, thus the models produced from QP inversion (Fig. 9a) show more variations (are less smoothed) than models resulted from SVD (e.g. Fig. 5d).

To assess the resolution and reliability of the model obtained, various synthetic tests were also conducted. Synthetic data corresponding to the model obtained from the inversion as shown in Fig. 5(d) were generated using the same ray geometry as for the real data. In the examples shown here, Gaussian noise with standard deviation equal to 0.1 s was added to the synthetic data sets and the synthetic data were then inverted using the same inversion parameters (i.e. block size, damping, etc.) as used for the real data.

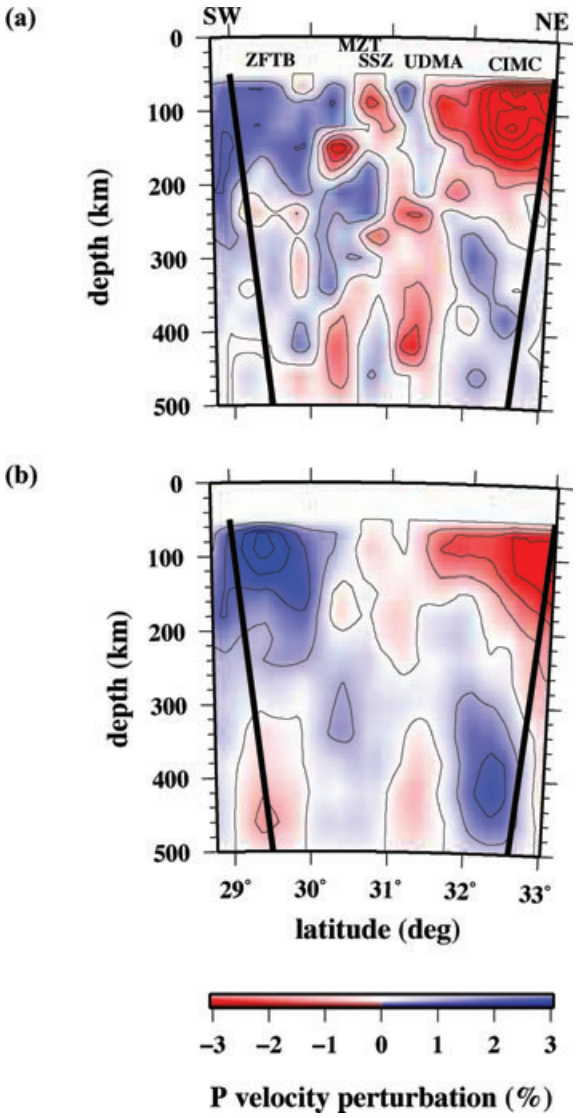

Figure 9. A cross-section along the studied profile for (a) inversion result based on quadratic programming method and (b) synthetic test inversion result (the input model is shown in Fig 5d).

The corresponding resolved image at the third iteration is shown in Fig. 9(b). Based on the synthetic test, it can be concluded that the positions of the major structures seen in the real data are resolved well by the data set, although the absolute values of the velocity perturbations are not fully recovered in the inversion which can be due to different regularization parameters such as damping.

Checkerboard tests are commonly used to assess solution quality in teleseismic tomography studies. Synthetic data corresponding to the checkerboard test models shown in Fig. 10 (left-hand columns) were generated using the same ray geometry as for the real data. Gaussian noise with standard deviation equal to 0.1 s was added to the synthetic data. The inversions results after the third iterations are shown in Fig. 10 (right-hand columns).

Resolution tests using the inversion results as an input model to calculate synthetic traveltime data (e.g. Fig. 9b) may have some drawbacks that areas of low resolution are identified as areas of good resolution due to the good recovery of the input model, which either shows low-amplitude anomalies or even artefacts in areas of low resolution (e.g. Husen *et al.* 2003). Checkerboard tests give only good estimates of the amount of smearing. The ability of the data to resolve fine-scale chequerboard structures does not necessarily imply that large-scale structures are resolved as well (e.g. Lévêque *et al.* 1993; Husen *et al.* 2003). Thus, to assess the reliability of the inversion result, we decided to combine the results of different measures as discussed earlier. By comparing various resolution analyses presented in Figs 9 and 10 it can be concluded that at the central part of the profile (30.5–32° and depth of about 100–200 km) the resolution is low which is due to the limited amount of ray coverage (caused by the limited number of stations). Vertical smearing is observed in all the synthetic models presented. It is stronger in the upward direction than downwards due to the near-vertical nature of the teleseismic rays. However, the lateral resolution (especially around MZT) seems to be very good and it is in the order of 50 km. The size of the network allows inversion for structures even at greater depths, and lateral variations of velocity at depths of up to 460 km appear to be resolved. For instance, the existence of the north-dipping slab-like positive velocity anomaly is well resolved by applying the resolution analyses carried out in this study. Based on various synthetic tests done for the Zagros experiment and also based on observed data uncertainties (estimated from weighting factors assigned in phase-picking process), low-amplitude anomalies less than ±0.5 per cent cannot be considered to be resolved. A possibility remains that while the features are not caused by the inversion algorithm as such, they are artefacts due to the fundamental character of the data, including possible noise. However, our various resolution tests and the use of independent inversion algorithms strongly suggest that the major features seen in the inverted images do represent significant lateral velocity variations at depth.

7 DISCUSSION

The most important factor influencing seismic velocity in the upper mantle is probably attributed to variations in temperature (Goes *et al.* 2000). The often cited alternatives that are used to explain the velocity variations in the upper mantle are composition, presence of partial melt, the presence of water and anisotropy due to lattice preferred orientation (e.g. Goes *et al.* 2000; Hieronymus *et al.* 2007). The Arabian plate is expected to be relatively cold in contrast to the Central Iran, because high-velocity anomalies in the upper mantle may mark the presence of stable, cold and thick lithospheric mantle. Therefore much of the 3-D mantle velocity structure in the upper mantle along the Zagros profile can be attributed to the thermal effects. However, although the direct effect of composition on seismic velocity is minor, its effect on viscosity is crucial in stabilizing the lithospheric system. Therefore, the observed variations in seismic velocity can be considered as an indirect result of the compositional differences. Mantle convection and other dynamic effects (e.g. slab dehydration) are probably common factors which control the features of the continental lithospheric system in the studied area (e.g. Arcay *et al.* 2005; Hieronymus *et al.* 2007).

We have assumed an isotropic velocity structure. The presence of anisotropy may bias isotropic velocity estimates where waves sample predominantly in one direction (Goes *et al.* 2000). Information on magnitude and orientation of anisotropy along the profile is limited. However, our results may be biased by the presence of anisotropy. In the Zagros experiment, the propagation directions of the incoming *P* phases span only a limited range of azimuth (±10°) and in dip (±30°) due to the near-vertical incident angles of the teleseismic rays. Thus, for a given cell, the velocity difference will not be larger than 0.7 per cent for a simple transverse anisotropy

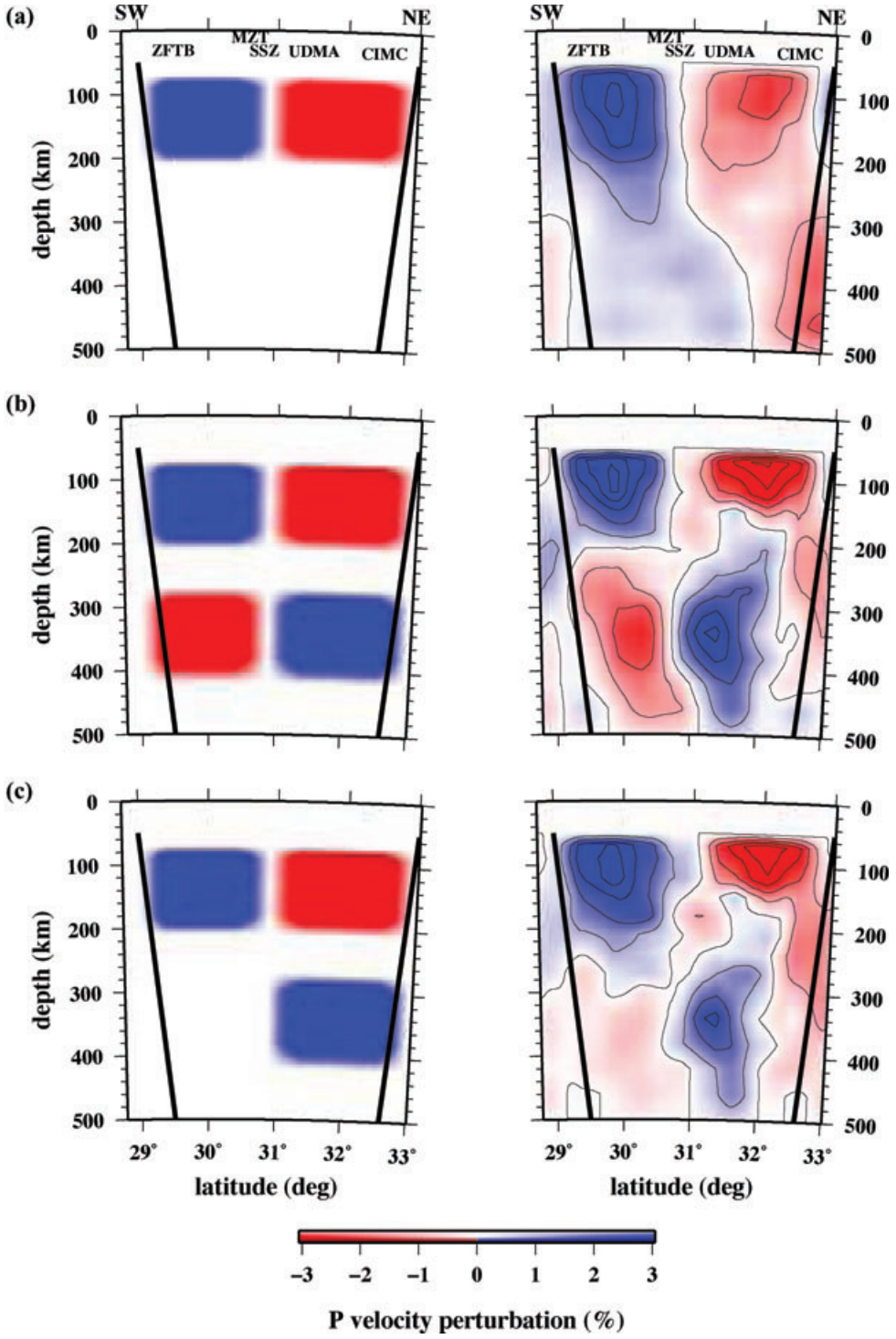

Figure 10. Checkerboard test showing synthetic models (left-hand columns) and model results (right-hand columns). Different possible scenarios are shown as velocity anomalies are only located in (a) uppermost mantle, (b) in the upper 400 km of the model and (c) for a NE-dipping slab-like structure. Tectonic abbreviations as in Fig. 1.

system with 4 per cent anisotropy. Therefore, interpreting the image in terms of average (isotropic) velocities may be misleading if strong anisotropy is present. The size of the observed anomalies suggests that bulk changes in velocity are required by the data, even if there may be some contribution from anisotropy.

Our tomography model (Fig. 5d) reveals a rather discontinuous decrease in *P* velocity from south to north along the Zagros profile. The existence of a major near-vertical lateral change in *P* velocity of several per cent to depths of 250 km essentially below the Zagros collision zone at about 30°N is a structure resolved in different inversions carried out. The transition coincides with the MZT at the Earth's surface (Fig. 1). The Arabian Shield (ZFTB) is characterized by thick lithosphere, whereas, the Central Iran in the northern part of the profile is almost devoid of a shield-like mantle lithosphere. The low upper-mantle velocities (seen at the northern part of the profile) suggest a warmer than normal upper

mantle (Jackson 2000) but do not necessarily indicate presence of partial melt (Priestley & McKenzie 2002). This result is consistent with previous surface wave tomographic studies in the Middle East which have documented lower *S*-wave velocities at 100 km depth beneath Central Iran than beneath the Arabian platform (Debayle *et al.* 2001; Shapiro & Ritzwoller 2002; Maggi & Priestley 2005) and also body-wave tomography studies (e.g. Kaviani *et al.* 2007).

The most striking feature resolved in the central part of the model (30.5–33°N) is a steeply north-dipping slab-like positive velocity anomaly that plunges under the anomalously low relative velocity upper-mantle structure of Central Iran. This structure fits the upper part of the cold seismic curtain shown by Hafkenscheid *et al.* (2006) underneath the Zagros collision system. As Fig. 5(d) shows, this positive anomaly branches off from the shield-like upper mantle of ZFTB at about 30.5° latitude and depth of about 200 km. This feature is approximately 100 km thick and continues underneath UDMA and Central Iran to depths of more than 400 km. Due to the limited resolution of the data, this apparently continuous 'slab' could in fact be due to two or more spatially separate anomalies, notwithstanding, we tentatively interpret this structure as an aseismic remnant slab. Using partitioned waveform inversion method across the Zagros collision zone Shad Manaman *et al.* (2011) showed that the slab does not penetrate the transition zone and deflects at about 410 km depth, giving rise to a horizontal high-velocity anomaly observed in the tomographic images. In addition it is also documented that the absence of deep seismicity in the Benioff zone does not indicate the absence of a subducted slab. There are many well-known subduction zones, for example, the Aegean slab and Izu-Bonin slab, with no association with deep Benioff seismicity (Wortel *et al*. 1990; Brudzinski *et al.* 2005; Shad Manaman *et al.* 2011). Alternatively, this feature could represent delamination of the lower lithosphere of the Zagros continental block that is detached from its crust following the collisional convergence (Stern *et al.* 2000). Predictably, the same structure for the upper mantle including a fragment of the subducted lithosphere has been resolved across the Zagros collision zone using surface wave tomography (Shad Manaman & Shomali 2010; Shad Manaman *et al.* 2011) and *S*-phase teleseismic tomography (Keshvari *et al.* 2011) studies.

The negative velocity anomaly characterizing the upper mantle of Iran north of the MZT has been widely documented (e.g. Kaviani *et al.* 2007; Shad Manaman & Shomali 2010), however, its southward extension is either uncertain (Paul *et al.* 2006; Kaviani *et al.* 2007) or has been shown with little details (Bijwaard *et al.* 1998; Bijwaard & Spakman 2000). Our high-resolution tomography results enable us to show that the pronounced low-velocity anomaly beneath UDMA which fades southwards beneath the Sanandaj-Sirjan zone reappears with less intensity underneath the ZTZ and continues to depths of about 200 km and between latitudes of 30.5° and 31° (Fig. 5d). This feature seems to be indicating delamination of the mantle lid from the lower crust in the ZTZ and upwelling of the asthenosphere through the ruptured slab, as it is pulling off from the Arabian mantle lithosphere, though we are aware that due to the limited resolution of the data, the positions and robustness of these small anomalies are not quite well supported by the data.

This finding is at odds with previous interpretations that the northeastern edge of the Arabian plate has a shield-like *P*-wave velocity structure (e.g. Kaviani *et al.* 2007), and if the lower crust of the ZTZ is indeed in juxtaposition with the asthenosphere then certain consequences are expected. Below we discuss the nature of the support for high topography and outlook of post-collisional magmatism.

A peculiar observation is that the High Zagros is not underlain by the thickest crust (Fig. 5). The average Moho depth is 45–50 km beneath the folded belt (Hatzfeld *et al.* 2003; Paul *et al.* 2006). It deepens rather abruptly beneath the MZT and the SSZ. The maximum crustal thickness of about 65 km is attained 50 km NE of the surface trace of the MZT. In other words the region of overthickened crust is shifted to the NE with respect to the areas of highest elevations (Fig. 5c) and the strongest negative Bouguer anomaly (Paul *et al.* 2006). It is essential to note that our cross-section runs through the 'High Zagros' which is a 700-km-long by 50–100-km-wide segment in the central and western ZTZ and attains an average elevation of about 3–3.5 km with numerous peaks above 4 km elevation. We suggest that the high elevation in the ZTZ is supported by hot asthenosphere rather than a thickened crust. Post-collisional asthenospheric upwelling has similarly been applied for explaining what supports the high topography in the East Anatolian Plateau (Şengör *et al.* 2003). This thermal event may also be related to the enigmatic post-Miocene regional uplift in the Zagros fold belt (Mouthereau *et al.* 2006).

A nearby and better studied example of the phenomenon mentioned is the East Anatolian Plateau that exhibits widespread post-collisional volcanism (e.g. Keskin 2003). Similarly, areas to the north of the MZT display volcanic activity with products which are mafic alkaline, that is, compositionally distinct from the older subduction related rocks. Volcanism related to post-Early Miocene evolution of Iran has been documented in southeastern UDMA (Hassanzadeh 1994) and SSZ (Boccaletti *et al.* 1976).

8 CONCLUSIONS

(1) According to the model presented in this study (see Fig. 5d) a general discontinuous decrease in *P* velocities in the upper mantle from south to north is resolved by the data. In the Arabian Shield, thick continental lithosphere (more than 200 km) is seen in the southern part of the profile. The model presented indicates no (or very thin) lithospheric mantle under the northern part of the model (i.e. Central Iran). Abrupt lateral *P*-velocity changes (maximum 6 per cent) are seen at both the southern and northern sides of the ZTZ. The existence of a major near-vertical lateral change in *P* velocities of several per cent to depths of about 250 km more or less directly below the MZT is a common feature resolved in the various inversions carried out. Thus according to our results, the transition between Arabia and Central Iran can be postulated to coincide with the MZT at the surface (Fig. 1).

(2) Our results (see Fig. 5d) indicate the presence of a disconnected cold northeast dipping oceanic slab or detached mantle lithosphere beneath Central Iran.

(3) Our high-resolution tomography also points to lithospheric delamination underneath the ZTZ. This model observation is supported by independent evidence. Despite its highest elevation, the ZTZ is not underlain by the thickest crust along the investigated traverse. This implies that the high elevation in the ZTZ is supported by shallow asthenosphere replacing the peeled off mantle lithosphere.

ACKNOWLEDGMENTS

Seismological data used in this paper were retrieved from the data management centre of the French portable seismic instrument pool hosted by LGIT (Grenoble University-CNRS), http://bdsis.obs.ujf-grenoble.fr/. We thank C. Péquegnat and H. Pedersen (LGIT

Grenoble) for their valuable help. Some figures were made using the Generic Mapping Tools (GMT) version 4.2.1 (Wessel & Smith 1998; www.soest.hawaii.edu/gmt, last accessed 2010 August). We would also like to thank the Associate Editor, Gabi Laske, and four anonymous reviewers for their constructive comments and useful suggestions. We also thank Roland Roberts (Department of Earth Sciences, Uppsala University, Sweden) and Faramarz Tutti (Department of Geology, University of Tehran, Iran) for their valuable comments on the manuscript.

REFERENCES

Aki, K., Christoffersson, A. & Husebye, E., 1977. Determination of the three-dimensional seismic structure of the lithosphere, *J. geophys. Res.*, **82,** 277–296.

Arcay, D., Tric, E. & Doin, M.-P., 2005. Numerical simulations of subduction zones: effect of slab dehydration on the mantle wedge dynamics, *Phys. Earth planet. Inter.*, **149,** 133–153.

Arlitt, R., 1999. Teleseismic body wave tomography across the Trans-European Suture Zone between Sweden and Denmark, *PhD thesis,* ETH, Zürich.

Bassin, C., Laske, G. & Masters, G., 2000. The current limits of resolution for surface wave tomography in North America, *EOS, Trans. Am. geophys. Un.*, **81,** F897.

Bijwaard, H. & Spakman, W., 2000. Nonlinear global *P*-wave tomography by iterated linearized inversion, *Geophys. J. Int.*, **141,** 71–82.

Bijwaard, H., Spakman, W. & Engdahl, E.R., 1998. Closing the gap between regional and global travel time tomography, *J. geophys. Res.*, **103,** 30 055–30 078.

Boccaletti, M., Innocenti, F., Manetti, P., Mazzuoli, R., Motamed, A., Pasquare, G., Radicati di Brozolo, F. & Amin Sobhani, E. 1976. Neogene and quaternary volcanism of Bijar area (western Iran), *Bull. Volcanologique*, **40**(2), 121–132.

Brudzinski, M.R., Chen, W., Pillet, R. & Tseng, T., 2005. Connecting active subduction to aseismic remnant slabs: evolution of petrologic anomalies in the mantle transition zone, *EOS, Trans. Am. geophys. Un.*, Fall Meeting Abstract DI41A-1262.

Debayle, E., Leveque, J.-J. & Cara, M., 2001. Seismic evidence for a deeply rooted low-velocity anomaly in the upper mantle beneath the northeastern Afro-Arabian continent, *Earth planet. Sci. Lett.*, **193,** 423–436.

Dueker, K., Humphreys, E. & Biasi, G., 1993. Teleseismic imaging of the western United States upper mantle structure using the simultaneous iterative reconstruction technique, in *Seismic Tomography: Theory and Practice*, pp. 265–298, eds Iyer, H.M. & Hirahara, K., Chapman & Hall, London.

Eken, T., Shomali, H., Roberts, R. & Bödvarsson, R., 2007. Upper mantle structure of the Baltic shield below the Swedish National Seismological Network (SNSN) resolved by teleseismic tomography, *Geophys. J. Int.*, **169,** 617–630, doi: 10.1111/j.1365-246X.2007.03351.x.

Eken, T., Shomali, Z.H., Roberts R., Hieronymus, C.F. & Bodvarsson, R., 2008. *S* and *P* velocity heterogeneities within the upper mantle below the Baltic Shield, *Tectonophysics*, **462,** 109–124, doi:10.1016/j.tecto.2008.02.015.

Engdahl, E.R., Van der Hilst, R.D. & Buland, R.P., 1998. Global teleseismic earthquake relocation with improved travel times and procedures for depth determination, *Bull. seism. Soc. Am.*, **88,** 722–743.

Engdahl, E.R., Jackson, J.A., Myers, S.C., Bergman, E.A. & Priestley, K., 2006. Relocation and assessment of seismicity in the Iran region, *Geophys. J. Int.*, **167,** 761–778.

Evans, J. & Achauer, U., 1993. Teleseismic velocity tomography using the ACH method: theory and application to continental-scale studies, in *Seismic Tomography: Theory and Practice*, pp. 319–360, eds Iyer, H.M. & Hirahara, K., Chapman & Hall, London.

Goes, S., Govers, R. & Vacher, P., 2000. Shallow mantle temperatures under Europe from *P* and *S* wave tomography, *J. geophys. Res.*, **105,** 11 153–11 169.

Hafkenscheid, E., Wortel, M.J.R. & Spakman, W., 2006. Subduction history of the Tethyan region derived from seismic tomography and tectonic reconstructions, *J. geophys. Res.*, **111,** B08401, doi:10.1029/2005JB003791.

Hassanzadeh, J., 1994. Consequence of the Zagros continental collision on the evolution of the central Iranian plateau, *J. Earth Space Phys.*, **21,** 27–38 (in Persian, with English abstract).

Hatzfeld, D., Tatar, M., Priestley, K. & Ghafory-Ashtyany, M., 2003. Seismological constraints on the crustal structure beneath the Zagros mountain belt (Iran), *Geophys. J. Int.*, **155,** 403–410.

Hieronymus, C.F., Shomali, Z.H. & Pedersen, L.B., 2007. A dynamical model for generating sharp seismic velocity contrasts underneath continents: application to the Sorgenfrei-Tornquist Zone, *Earth planet. Sci. Lett.*, **262,** 77–91, doi:10.1016/j.epsl.2007.07.043.

Husen, S., Quintero, R., Kissling, E. & Hacker, B., 2003. Subduction-zone structure and magmatic processes beneath Costa Rica constrained by local earthquake tomography and petrological modelling, *Geophys. J. Int.*, **155,** 11–32.

Jackson, I., 2000. Laboratory measurements of seismic wave dispersion and attenuation: recent progress, *Am. geophys. Un. Monogr.*, **117,** 265–289.

Kadinsky-Cade, K. & Barazangi, M., 1982. Seismotectonics of southern Iran: the Oman Line, *Tectonics*, **1,** 389–412.

Kaviani, A., Paul, A., Bourova, E., Hatzfeld, D., Pedersen, H. & Mokhtari, M., 2007. A strong seismic velocity contrast in the shallow mantle across the Zagros collision zone (Iran), *Geophys. J. Int.*, **171,** 399–410.

Kennett, B.L.N. & Engdahl, E.R., 1991. Travel times for global earthquake location and phase identification, *Geophys. J. Int.*, **105,** 429–465.

Keshvari, F., Shomali, Z.H., Tatar, M. & Kaviani, A., 2011. Upper-mantle *S*-velocity structure across the Zagros collision zone resolved by nonlinear teleseismic tomography, *J. Seismol.*, **15,** 329–339, doi:10.1007/s10950-011-9226-y.

Keskin, M., 2003. Magma generation by slab steepening and breakoff beneath a subduction-accretion complex: an alternative model for collision-related volcanism in Eastern Anatolia, Turkey, *Geophys. Res. Lett.*, **30,** 8046, doi:10.1029/2003GL018019.

Koyi, H.A., 1988. Experimental modeling of the role of gravity and lateral shortening in the Zagros mountain belt, *AAPG Bull.*, **72,** 1381–1394.

Lawrence Livermore National Laboratory, 2010. *SAC: Seismic Analysis Code*, www.iris.edu/manuals/sac/manual.html (last accessed 2010 November).

Lévêque, J.J. & Masson, F., 1999. From ACH tomographic models to absolute velocity models, *Geophys. J. Int.*, **137,** 621–629.

Lévêque, J.-J., Rivera, L. & Wittlinger, G., 1993. On the use of the checkerboard test to assess the resolution of tomographic inversions, *Geophys. J. Int.*, **115,** 313–318.

Lippitsch, R., Kissling, E. & Ansorge, J. 2003. Upper mantle structure beneath the Alpine orogen from high-resolution teleseismic tomography, *J. geophys. Res.*, **108**(B8), 2376, doi:10.1029/2002JB002016.

Maggi, A. & Priestley, K., 2005. Surface waveform tomography of the Turkish-Iranian plateau, *Geophys. J. Int.*, **160,** 1068–1080.

Maggi, A., Jackson, J.A., Priestley, K. & Baker, C., 2000. A re-assessment of focal depth distributions in southern Iran, the Tien Shan and northern India: do earthquakes really occur in the continental mantle?, *Geophys. J. Int.*, **143,** 629–661.

Masson, F. & Trampert, J., 1997. On ACH, or how reliable is regional teleseismic delay time tomography?, *Phys. Earth planet. Inter.*, **102,** 21–32.

Moores, E. & Twiss, T., 1995. *Tectonics*, W.H. Freeman, New York, NY.

Mouthereau, F., Lacombe, O. & Meyer, B., 2006. The Zagros folded belt (Fars, Iran): constraints from topography and critical wedge modelling, *Geophys. J. Int.*, **165,** 336–356.

Nowroozi, A., 1971. Seismotectonics of the Persian plateau, eastern Turkey, Caucasus and Hindu Kush regions, *Bull. seism. Soc. Am.*, **61,** 317–341.

Oliver, J. & Murphy, L., 1971. WWNSS: seismology's global network of observing stations, *Science*, **174,** 254–261.

Parker, R.L., 1980. The inverse problem of electromagnetic induction: existence and construction of solutions based on incomplete data, *J. geophys. Res.*, **85,** 4421–4428.

Paul, A., Kaviani, A., Hatzfeld, D., Vergne, J. & Mokhtari, M., 2006. Seismological evidence for crustal-scale thrusting in the Zagros mountain belt (Iran), *Geophys. J. Int.*, **166,** 227–237.

Powell, M.J.D., 1983. On the Quadratic Programming Algorithm of Goldfarb and Idnani, Report DAMTP 1983 /Na 19, University of Cambridge, Cambridge.

Priestley, K. & McKenzie, D., 2002. The structure of the upper mantle beneath southern Africa, *Geol. Soc. Lond. Spec. Publ.,* **199,** 45–64, doi:10.1144/GSL.SP.2002.199.01.03.

Sandoval, S., Kissling, E., Ansorge, J. & the SVEKALAPKO STWG, 2004. High-resolution body wave tomography beneath the SVEKALAPKO array: II. Anomalous upper mantle structure beneath central Baltic schield, *Geophys. J. Int.*, **157,** 200–214. doi:10.1111/j.1365-246X.2004.02131.x

Schittkowski, K., 2000. *Fortran Subroutine*, Math. Institut. Universitaet Bayreuth.

Şengör, A.M.C., Özeren, S., Genç, T. & Zor, E., 2003. East Anatolian high plateau as a mantle-supported, north-south shortened domal structure, *Geophys. Res. Lett.*, **30,** 8045, doi:10.1029/2003GL017858.

Shad Manaman, N. & Shomali, H., 2010. Upper mantle *S*-velocity structure and Moho depth variations across Zagros belt, Arabian–Eurasian plate boundary, *Earth planet. Inter.*, **180,** 92–103.

Shad Manaman, N., Shomali, H. & Koyi, H., 2011. New constraints on upper-mantle *S*-velocity structure and crustalthickness of the Iranian plateau using partitioned waveform inversion, *Geophys. J. Int.*, **184,** 247–267. doi:10.1111/j.1365-246X.2010.04822.x.

Shapiro, N.M. & Ritzwoller, M.H., 2002. Monte-Carlo inversion for a global shear-velocity model of the crust and upper mantle, *Geophys. J. Int.*, **151,** 88–105.

Shomali, Z.H., Roberts, R.G. & the TOR Working Group, 2002. Non-linear body wave teleseismic tomography along the TOR array, *Geophys. J. Int.*, **148,** 562–575.

Shomali, Z.H., Roberts, R.G., Pedersen, L.B. & the TOR Working Group, 2006. Lithospheric structure of the Tornquist Zone resolved by nonlinear *P* and *S* teleseismic tomography along the TOR array, *Tectonophysics*, **416,** 133–149, doi:10.1016/j.tecto.2005.11.019.

Stammler, K., 1993. Seismic Handler-Programmable multichannel data handler for interactive and automatic processing of seismological analyses, *Comput. Geosci.*, **2,** 135–140.

Stampfli, G.M. & Borel, G.D., 2004. The TRANSMED transects in space and time: constraints on the paleotectonic evolution of the mediterranean domain, in *The TRANSMED Atlas: The Mediterranean Region from Crust to Mantle*, pp. 53–80, eds Cavazza, W., Roure, F., Spakman, W., Stampfli, G.M. & Ziegler, P., Springer-Verlag, Berlin.

Steck, L.K. & Prothero, W.A., Jr., 1991. A 3-D raytracer for teleseismic body-wave arrival times, *Bull. seism. Soc. Am.*, **81,** 1332–1339.

Stern, T., Molnar, P., Okaya, D. & Eberhart-Phillips, D., 2000. Teleseismic *P*-wave delays and modes of shortening the mantle lithosphere beneath South Island, New Zealand, *J. geophys. Res.*, **105,** 21 615–21 631.

Stöcklin, J., 1968. Structural history and tectonics of Iran: a review, *Am. Assoc. Pet. Geol. Bull.*, **52,** 1229–1258.

Weiland, C.M., Steck, L.K., Dawson, P.B. & Korneev, V., 1995. Nonlinear teleseismic tomography at Long Vally caldera, using three-dimensional travel time ray tracing, *J. geophys. Res.*, **100,** 20 379–20 390.

Wessel, P. & Smith, W.H.F., 1998. New, improved version of generic mapping tools released, *EOS, Trans. Am. geophys. Un.*, **79,** 579.

Wortel, M.J.R., Goes, S.D.B. & Spakman, W., 1990. Structure and seismicity of the Aegean subduction zone, *Terra Nova*, **2**(6), 554–562.